Inorganic Chemistry

Article

pubs.acs.org/IC

1,1′-Bis(pyrazol-3-yl)ferrocene: A Clip Ligand That Forms Supramolecular Aggregates and Prismatic Hexanuclear Coinage Metal Complexes

Mattia Veronelli, Sebastian Dechert, Serhiy Demeshko, and Franc Meyer*

Institut für Anorganische Chemie, Georg-August-Universität Göttingen, Tammannstrasse 4, 37077 Göttingen, Germany

Supporting Information

ABSTRACT: Two ferrocene derivatives with appended pyrazole substituents, namely, 1,1′-bis(5-methyl-1*H*-pyrazol-3-yl)ferrocene (H_2L^H) and 1,1′-bis(5-trifluoromethyl-1*H*-pyrazol-3-yl)ferrocene (H_2L^F), were synthesized. In solid state they form distinct H-bonded dimers with orthogonal (H_2L^H, C_2 symmetry) or antiparallel (H_2L^F, C_{2h} symmetry) arrangement of the two ferrocene/pyrazole hybrid molecules. Supramolecular dimerization was also detected in solution at low temperatures, though diffusion-ordered spectroscopy and variable-temperature NMR spectroscopy revealed several dynamic processes. Redox potentials of the ferrocene derivatives are affected by the nature of the pyrazole substituent (Me, CF_3). In their deprotonated form $[L^R]^{2-}$, both ferrocene/pyrazole hybrids serve as ligands and form oligonuclear Cu^I, Ag^I, and Au^I complexes that were identified by matrix-assisted laser desorption ionization mass spectrometry. X-ray crystallography revealed the structures of $Cu_6L_3^H$ and $Ag_6L_3^F$, which both contain two parallel and eclipsed $[M(\mu\text{-pz})]_3$ metallamacrocycles (M = Cu, Ag) linked by three ferrocene units. $M^I\cdots M^I$ distances between the two triangular M_3N_6 decks are shorter in $Ag_6L_3^F$ (3.28−3.30 vs 3.44−3.51 Å in the case of $Cu_6L_3^H$), indicating substantial *intra*molecular closed-shell $Ag(d^{10})-Ag(d^{10})$ interactions. However, $Cu_6L_3^H$ features close *inter*molecular Cu···Cu contacts as short as 3.37 Å. Mössbauer data for both the ligands and complexes were collected, and electrochemical properties were measured; preliminary luminescence data are reported.

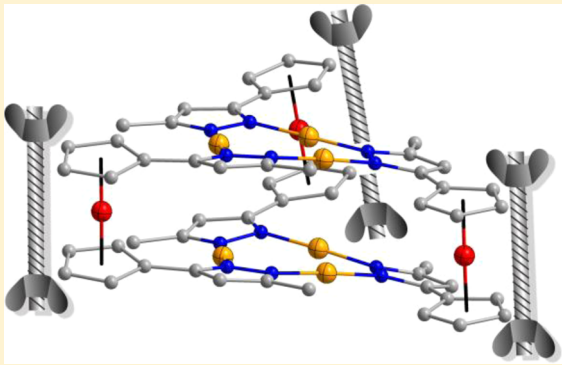

INTRODUCTION

Oligomeric complexes of monovalent coinage metals hold a prominent place in pyrazolate (pz) coordination chemistry.[1−3] Their most common structural motif is the trimeric $[M(\mu\text{-pz})]_3$ having a planar nine-membered metallomacrocycle with three Cu^I, Ag^I, or Au^I ions and three *N*,*N*′-bridging pz ligands, though polymeric, tetrameric, or hexameric compounds are also known.[2,4] Of particular interest is the aggregation of these triangular $[M(\mu\text{-pz})]_3$ via metallophilic $d^{10}-d^{10}$ interactions between the closed-shell M^I ions, which leads to fascinating supramolecular architectures and interesting photophysical properties.[5−12] From a supramolecular point of view the so-called "dimer of trimers" arrangement is often encountered in solid state (**I**, Figure 1),[8−10,13−16] but substituents at the pyrazole ring can have a decisive effect on the aggregation pattern.[17,18] Furthermore, substituents featuring additional donor sites can be used to decorate the cyclic coinage metal pz oligomers with additional metal ions,[11,12] and it was found that an additional Ag^I ion can be inserted between two $[M(\mu\text{-pz})]_3$ decks to give a sandwichlike heptametallic cluster.[19] To control and maximize the $d^{10}-d^{10}$ interactions between cyclic oligomers $[M(\mu\text{-pz})]_n$, some recent studies have introduced bis(pyrazolato) ligands with different linkers between the two diazole heterocycles.[20,21] This has allowed for the targeted synthesis of some hexanuclear complexes composed of stacked pairs of $[M(\mu\text{-pz})]_3$ trimers, either in the frontal (**II**) or staggered (**III**) modes. With proper spacing of the two decks such hexametallic nanocages can serve as hosts toward guest molecules such as S_8.[22]

Inspired by these developments, we decided to prepare a clip ligand in which two pyrazoles are connected by a ferrocene moiety instead of an organic linker and to study its ability to form type **II** hexanuclear coinage metal pyrazolates. Mono- and 1,1′-disubstitued ferrocene derivatives furnished with, for example, heterocycles such as pyridine, pyrimidine, pyrazine, quinoline, pyrazole, and triazole have previously been synthesized and used as ligands;[23] some of them were specifically designed for forming supramolecular assemblies via H-bonding.[24−26] Quite surprisingly, however, despite the well-established chemistry of pyrazole and ferrocene, only few reports about 1,1′-bis(pyrazolyl)-ferrocene have appeared in the literature, and its potential to serve as a ligand toward coinage metal ions seems unexplored so far.[27−31] Here we use two such proligands, namely, 1,1′-bis(5-methyl-1*H*-pyrazol-3-yl)ferrocene (H_2L^H; Chart 1), which was reported in 1961 by Cain et al. but never fully characterized,[28] and the new 1,1′-bis(5-trifluoromethyl-1*H*-pyrazol-3-yl)-ferrocene (H_2L^F). These two proligands and their complexes with Cu^I and Ag^I were studied both in solid state (via X-ray

Received: April 20, 2015
Published: June 26, 2015

DOI: 10.1021/acs.inorgchem.5b00898
Inorg. Chem. 2015, 54, 6917−6927

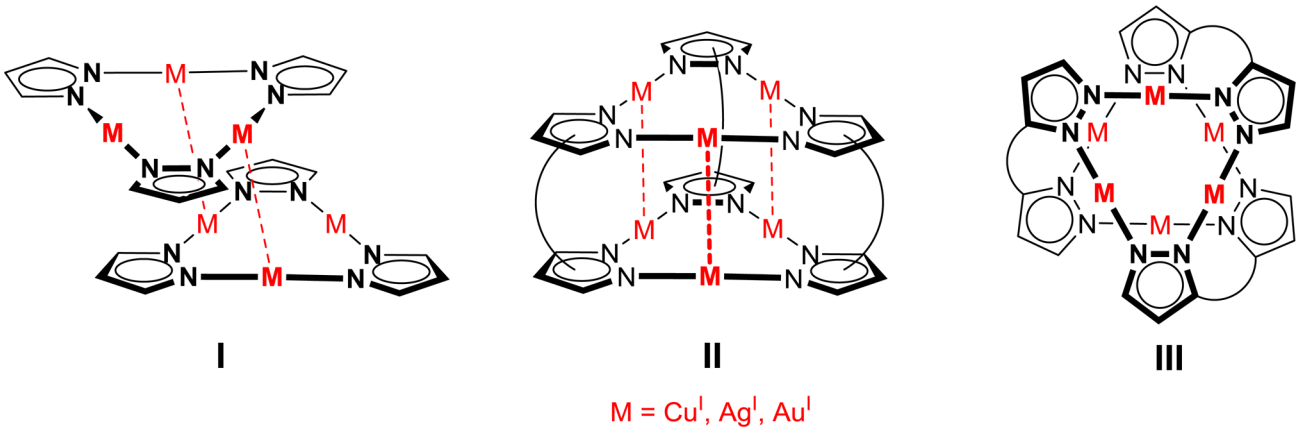

Figure 1. Dimer of trimers arrangement of coinage metal pyrazolates (**I**) and hexanuclear complexes composed of two cyclic trimers with bis(pyrazolato) clip ligands in the frontal (**II**) and staggered (**III**) modes.

Chart 1. Proligands H_2L^H and H_2L^F Described and Used in This Work

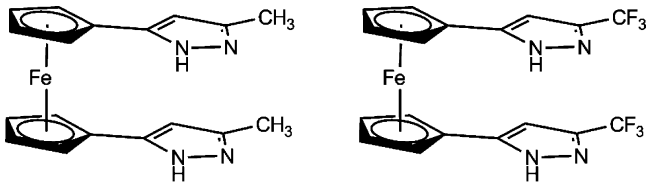

diffraction and Mössbauer spectroscopy) and in solution (NMR, cyclic voltammetry). Furthermore, preliminary luminescence data of the complexes are also reported.

RESULTS AND DISCUSSION

Ligands. The synthesis of the two ferrocene derivatives H_2L^H and H_2L^F with appended pyrazole groups was adapted from literature procedures (Scheme 1). 1,1′-Bisacetylferrocene, obtained from the reaction of acetyl chloride and ferrocene in the presence of $AlCl_3$,[32] was treated with EtONa and the appropriate ethyl ester to give the 1,1′-bis-β-diketone intermediates I^H and I^F, respectively, via Claisen condensation.[33] Formation of the pyrazole ring by reaction of I^H and I^F with hydrazine monohydrate finally yielded the target compounds.

For both proligands H_2L^H and H_2L^F it was possible to obtain single crystals suitable for X-ray diffraction. In both cases a syn-periplanar eclipsed conformation was found. While in H_2L^H the pyrazole rings are almost coplanar with interplanar angles in the range of 1.9°−10.6°, H_2L^F is more distorted with interplanar angles of the two pyrazoles between 15.5° and 25.0° (Supporting Information, Figures S21 and S22). Remarkably, both compounds crystallize as dimers that are held together by four hydrogen bonds, but their supramolecular structures are distinct (Figure 2). The arrangement of the four pyrazole rings that form the central core of the dimeric aggregate of H_2L^H resembles the one of common tetrameric pyrazoles, which usually adopt a saddle-like conformation.[34] Consequently each pyrazole ring of H_2L^H forms hydrogen bonds to both pyrazole rings of the second molecule H_2L^H, and the two ferrocene moieties are oriented in orthogonal directions. Approximately 1:1 disorder of the N-bound protons gives rise to crystallographic C_2 symmetry of the dimers $(H_2L^H)_2$.

In contrast, in the dimeric aggregate of H_2L^F two molecules are arranged in an antiparallel (head to tail) fashion with a "face to face" orientation of the pyrazoles. Therefore, pairs of pyrazole rings form two hydrogen bonds with each other, a motif that is also known from the solid-state structures of some simple pyrazole derivatives. Only one tautomeric form is observed for the pyrazole rings of $(H_2L^F)_2$, namely, with all NH groups next to the ferrocenyl substituents. This gives rise to noncrystallographic C_{2h} symmetry (crystallographic C_i symmetry) of the dimeric aggregate's core.

In solution at room temperature these types of supramolecular structures appear to be absent or to undergo dynamic processes that are rapid on the NMR time scale. ^{1}H NMR spectra of H_2L^H and H_2L^F (in deuterated dimethyl sulfoxide (DMSO-d_6), $CDCl_3$, or CD_2Cl_2) show only two signals associated with the cyclopentadienyl (Cp) rings, indicating that the ferrocenyl protons 2-H^{Fc} and 5-H^{Fc}, as well as 3-H^{Fc} and 4-H^{Fc}, are

Scheme 1. Synthesis of the Proligands H_2L^R

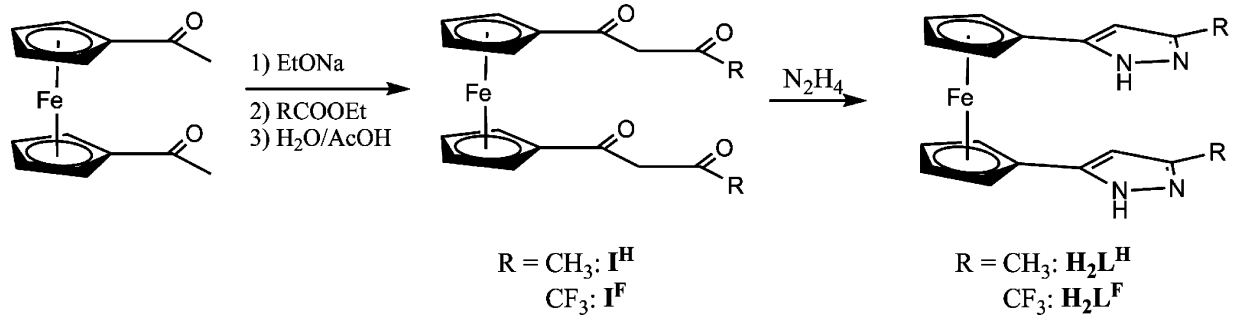

DOI: 10.1021/acs.inorgchem.5b00898
Inorg. Chem. 2015, 54, 6917−6927

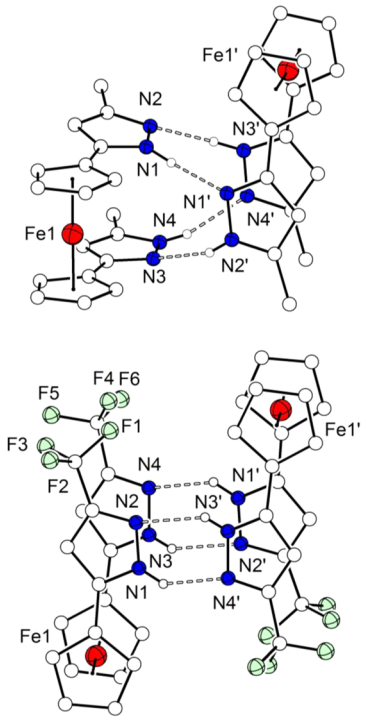

Figure 2. Supramolecular arrangement of H_2L^H (upper) and H_2L^F (lower) in solid state, emphasizing intermolecular hydrogen bonds (dashed lines) in the dimeric aggregates.

equivalent on the NMR time scale, that is, that rotation around the $1C^{Fc}-3C^{pz}$ bonds linking the ferrocene and pyrazole groups is fast. Besides, for H_2L^H the two pyrazole 4-H protons, CH^{pz}, give only a single peak, while they would be diastereotopic in a C_2-symmetric dimer such as the one found in solid state (in C_i or C_{2h} symmetric $(H_2L^F)_2$ dimers the CH^{pz} protons are homotopic anyway). However, the situation changes when ^{1}H NMR spectra are recorded at lower temperatures. In case of H_2L^H in CD_2Cl_2 solution it can be seen that the signal for the pyrazole H-4 splits into two broad resonances at ~250 K and, below 220 K, those two signals split again giving four singlets each integrating to one proton (Figure 3). Likewise the NH signal at low field and the signals for the Cp protons each split into four distinct resonances.

These spectra are in agreement with the formation, at temperature below 250 K, of dimers of H_2L^H, like the ones found in solid state and described above. In the intermediate temperature range, between 245 and 220 K, tautomerism of NH groups is still fast on the NMR time scale, and the averaged symmetric N···H···N bridges with protons halfway between the pyrazole-N atoms give rise to an apparent C_2 axis (Figure 4, left). At very low temperatures, even this tautomerism becomes slower than the NMR time scale, and the NH protons are now localized on a specific N atom; hence, the C_2 symmetry is lost, and all parts of the dimeric aggregate become inequivalent (Figure 4, right). Since the dimeric structure requires four hydrogen bonds to be held together, a conformation in which two NH are opposing each other is clearly impossible.

The proposed presence of dimers of H_2L^H at low temperatures was confirmed by means of ^{1}H diffusion-ordered spectroscopy (DOSY) NMR. Using the residual proton signal of CD_2Cl_2 as internal standard and recording spectra both at 293 and at 183 K it is in fact possible to demonstrate that, when cooled, the molecule in solution increases its volume by a factor of ~2.3 (for details of the calculation and ^{1}H DOSY see Supporting Information).

However, variable-temperature (VT) ^{1}H NMR of H_2L^F is clearly in disagreement with the formation, at low temperatures, of dimers with C_{2h} symmetry like the ones encountered in its crystal structure (Figure 2) for which a total of six signals is

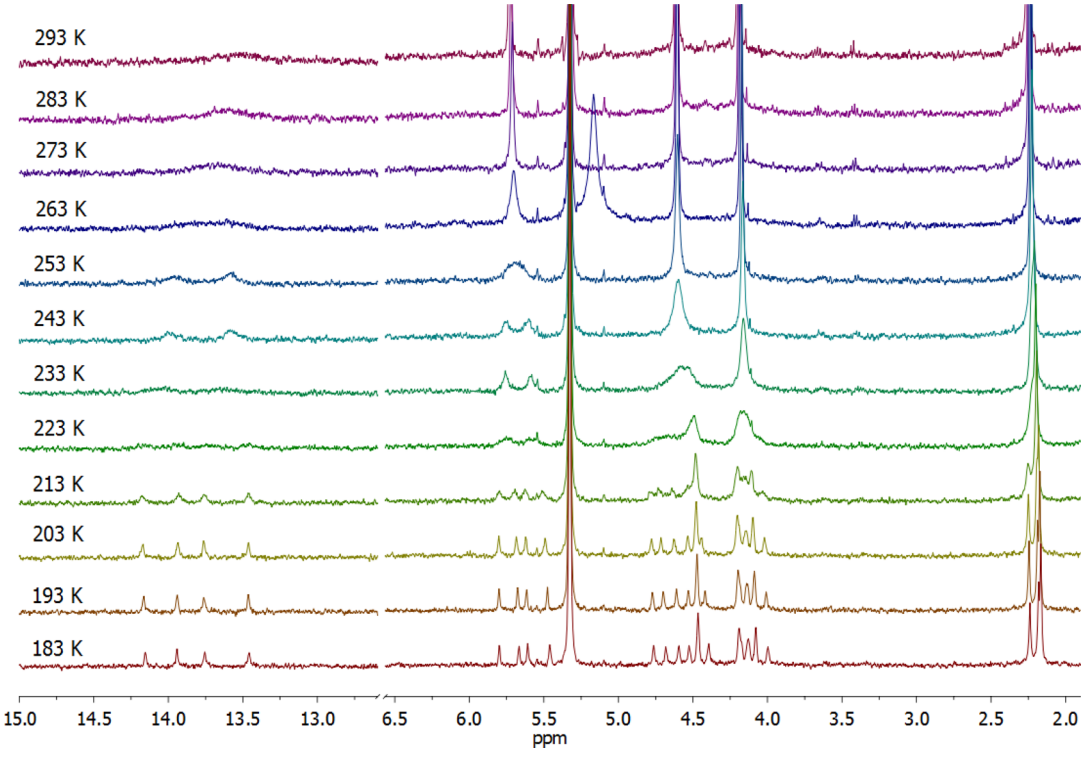

Figure 3. ^{1}H NMR spectra of H_2L^H recorded in CD_2Cl_2 at different temperatures.

DOI: 10.1021/acs.inorgchem.5b00898
Inorg. Chem. 2015, 54, 6917−6927

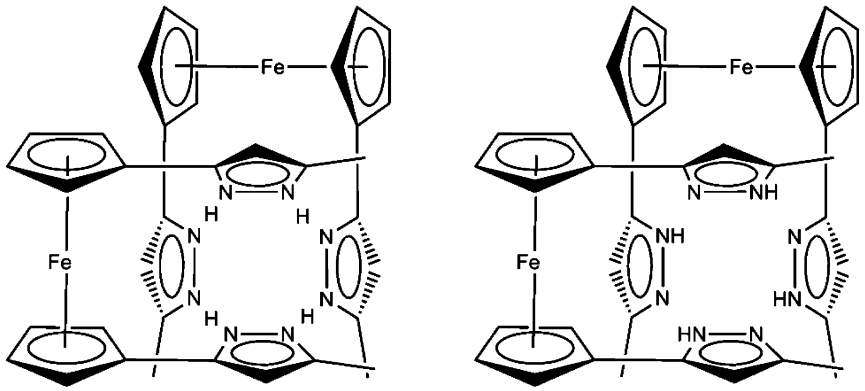

Figure 4. Schematic representation of the dimeric structure of H_2L^H present in solution: with apparent C_2 symmetry (between 245 and 220 K; left) and with frozen NH tautomerism (below 220 K; right).

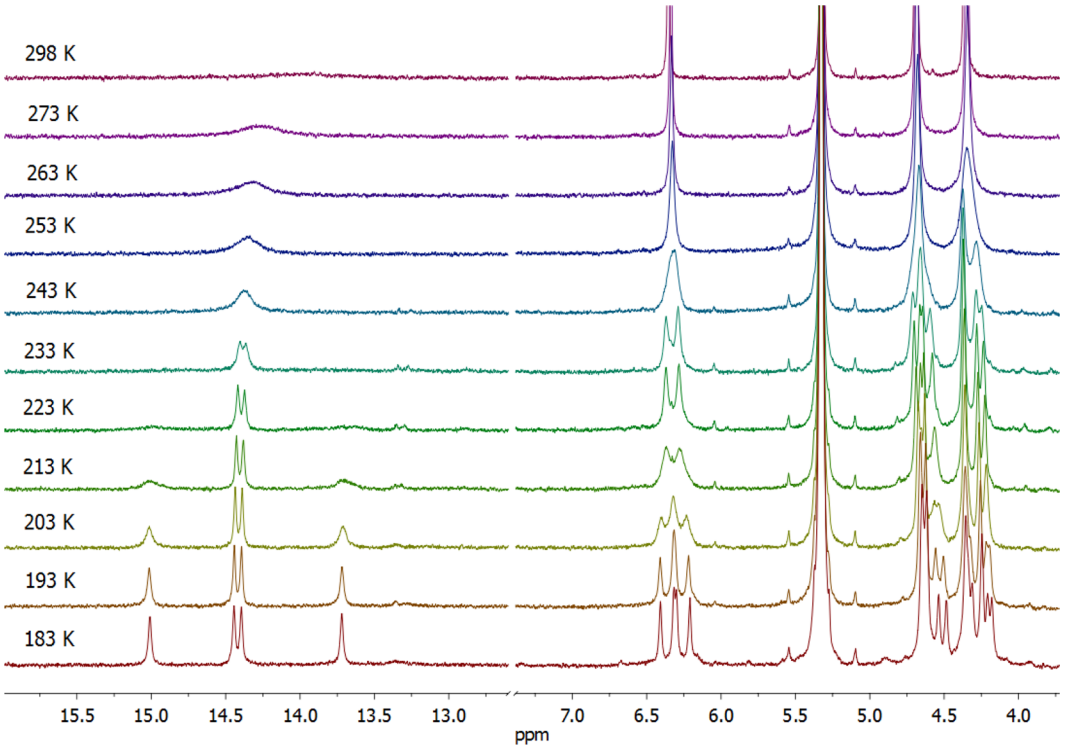

Figure 5. ^{1}H NMR spectra of H_2L^F recorded in CD_2Cl_2 at different temperatures.

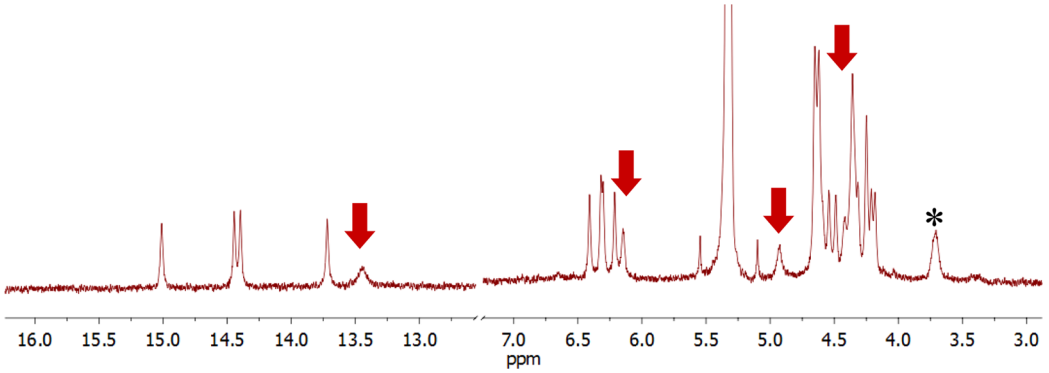

Figure 6. ^{1}H NMR spectrum of freshly dissolved crystalline material of H_2L^F recorded in CD_2Cl_2 at 183 K. The arrows indicate signals originating from the C_{2h} symmetric face-to-face dimer. The peak at 3.7 ppm marked with an asterisk is due to a minor impurity of EtOH.

expected in the absence of NH tautomerism (four for the Cp ring, one for 4-H^{pz}, and one for NH). However, the spectrum of H_2L^F resembles the one for H_2L^H as described above: when cooled, the peak for the pyrazole 4-H proton CH^{pz} splits into four

DOI: 10.1021/acs.inorgchem.5b00898
Inorg. Chem. 2015, 54, 6917−6927

new signals (two of them almost overlapping), each integrating to one, and the same is true for the NH resonances (Figure 5). The same pattern is also observed in the $^{19}F\{H\}$ NMR spectra, where a single signal is seen at 298 K that splits into four peaks at 183 K (Supporting Information, Figure S2). Remarkably, at low temperatures rotation of the CF_3 groups is slow enough, and F−F coupling through space is discernible, as demonstrated by ^{19}F COSY (Supporting Information, Figure S3). Finally, just as in the case of H_2L^H, ^1H DOSY supports the proposed dimerization of H_2L^F at low temperatures. Those observations led us to conclude that, for H_2L^F in solution, the formation of a C_2 symmetric dimer with the common saddle-shaped tetrameric ring of pyrazoles (i.e., a structure like the one of H_2L^H) is favored over the C_{2h} symmetric face-to-face dimer found in the solid state.

To detect the C_{2h} symmetric face-to-face dimers of H_2L^F in solution, crystalline material was dissolved in CD_2Cl_2 at −90 °C, and NMR spectra were recorded at the same temperature immediately afterward. As can be seen from Figure 6, rearrangement to the preferred C_2 symmetric core has largely occurred, but an additional set of pyrazole 4-H (CH^{pz}) and NH peaks is present, albeit broad (signals for the Cp protons of the two different dimeric forms partially overlap and cannot be easily distinguished). In ^{19}F NMR the signature is the same, and an additional peak assigned to the C_{2h} symmetric dimer is observed (Supporting Information, Figure S4). This indicates that at low temperatures H_2L^F can exist in two different dimer conformations, with the C_2 symmetric one (having the cyclic tetrameric pyrazole core) favored over the C_{2h} symmetric one.

Redox properties of the two ferrocene-derived ligands were investigated by means of cyclic voltammetry (CV) in dimethylformamide (DMF) and benzonitrile, using 0.1 M $[n\mathrm{Bu_4N}]PF_6$ as supporting electrolyte. In DMF, a reversible process was observed for H_2L^H with $E^0 = -0.05$ V versus Fc/Fc^+ (the dependence of peak separation ΔE_p on scan rate ν is due to uncompensated solution resistance under the experimental conditions), hence very close to the potential of parent ferrocene (Figure 7, upper). Oxidation of H_2L^F measured under the same conditions is chemically irreversible (Figure 7, middle). Even at rather high scan rates (300 mV s^{-1}) with a large anodic wave at $E_p^a = 246$ mV a peak in the reverse scan is barely visible; taking this weak cathodic signal with $E_p^c = 112$ mV gives a formal E^0 of +179 mV versus Fc/Fc^+. In contrast, in the less polar solvent benzonitrile, using ν = 100 mV s^{-1}, both H_2L^H and H_2L^F undergo reversible oxidation processes with $E^0 = -11$ mV and +215 mV, respectively (Figure 7, bottom, and Supporting Information, Figure S10). Obviously the nature of the remote substituent on the pyrazoles strongly affects the iron(II) center and the redox potential of the ferrocene backbone in H_2L^R species: as expected for a ferrocene derivative having substituents with electron-withdrawing CF_3-groups, E^0 of H_2L^F is shifted significantly by more than 200 mV toward positive potential compared to E^0 of parent Fc, and to H_2L^H with its Me substituents.

Complexes. The two bis(pyrazolyl)ferrocenes H_2L^H and H_2L^F were used as ligands toward copper(I) and silver(I). Direct reaction of H_2L^R with 2 equiv of the appropriate metal salt, namely, $[Cu(MeCN)_4](BF_4)$ or $AgBF_4$, in the presence of triethylamine leads to the formation of compounds of general formula $[M_2L^R]_x$ (M = Cu, Ag; x = 2, 3). The solvents used for these reactions were MeOH for the copper(I) complexes and MeCN (or a mixture MeCN/MeOH) for the silver(I) complexes, because the Ag/Ag^+ redox potential is much lower

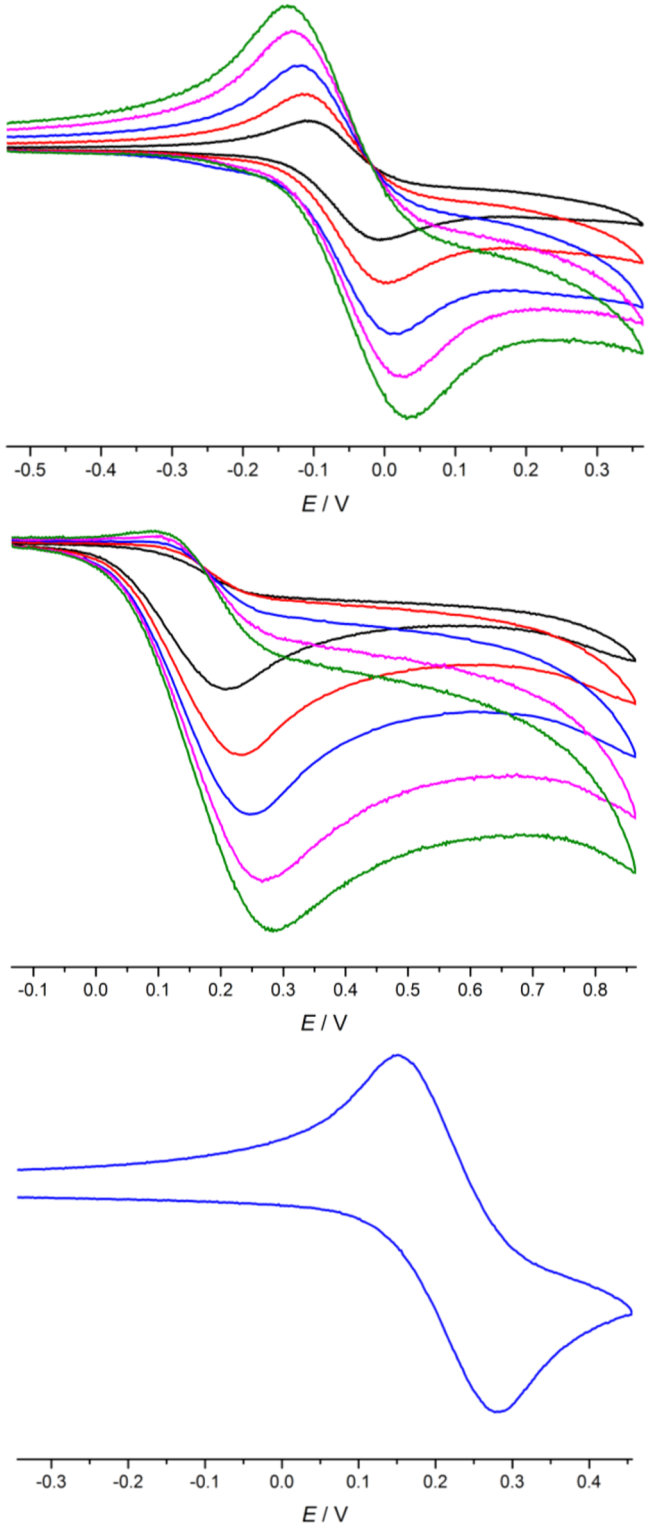

Figure 7. Cyclic voltammograms of H_2L^H (upper) and H_2L^F (middle) in DMF/0.1 M $[n\mathrm{Bu_4N}]PF_6$ vs Fc/Fc^+ at different scan rates (ν = 20, 50, 100, 200, 300 mV s^{-1}) (lower). Cyclic voltammogram of H_2L^F in PhCN/0.1 M $[n\mathrm{Bu_4N}]PF_6$ vs Fc/Fc^+ with scan rate of 100 mV s^{-1}.

in MeCN than in any other solvent,[35] and thus oxidation of the ferrocene unit by the silver(I) salt can be avoided.

The complexes $[M_2L^R]_x$ were first characterized using matrix-assisted laser desorption ionization time-of-flight mass spectrometry (MALDI-TOF-MS). For all but $[Cu_2L^F]_x$ a peak

DOI: 10.1021/acs.inorgchem.5b00898
Inorg. Chem. 2015, 54, 6917−6927

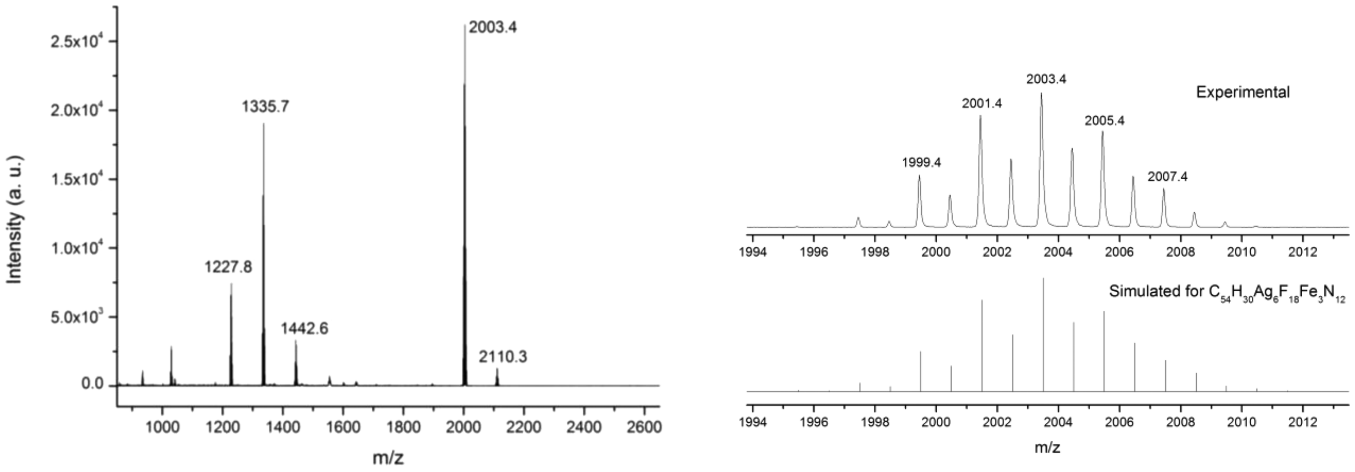

Figure 8. MALDI-TOF mass spectrum of $Ag_6L_3^F$ (left) with enlargement of the peak for the ion $[Ag_6L_3^F]^+$ (2003.4 m/z) and its simulated isotopic patter (right).

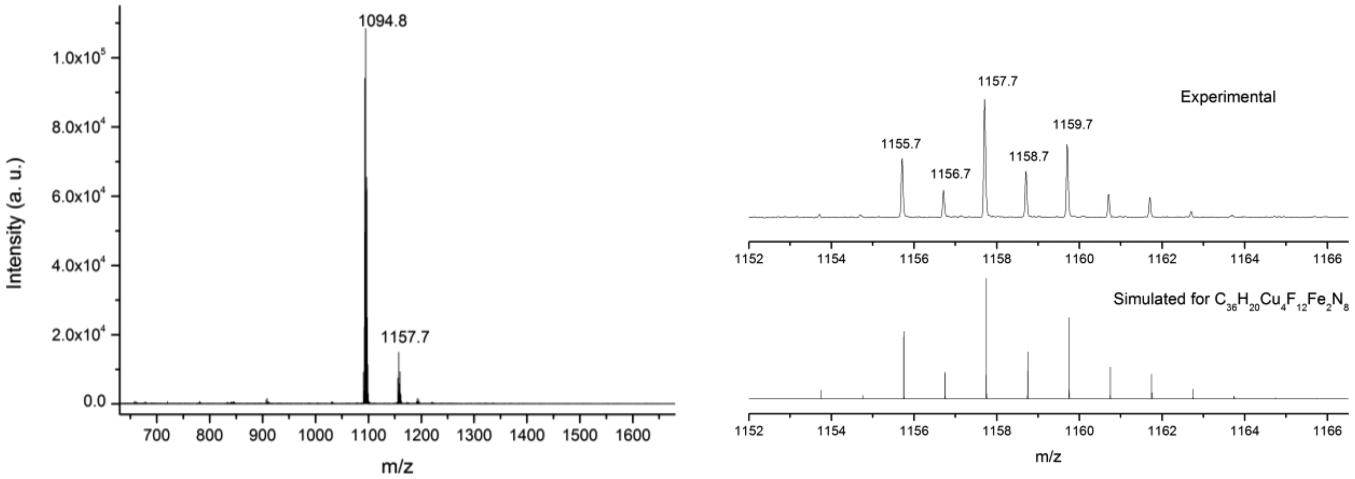

Figure 9. MALDI-TOF mass spectrum of $Cu_4L_2^F$ (left) with enlargement of the peak for the ion $[Cu_4L_2^F]^+$ (1157.7 m/z) and its simulated isotopic patter (right).

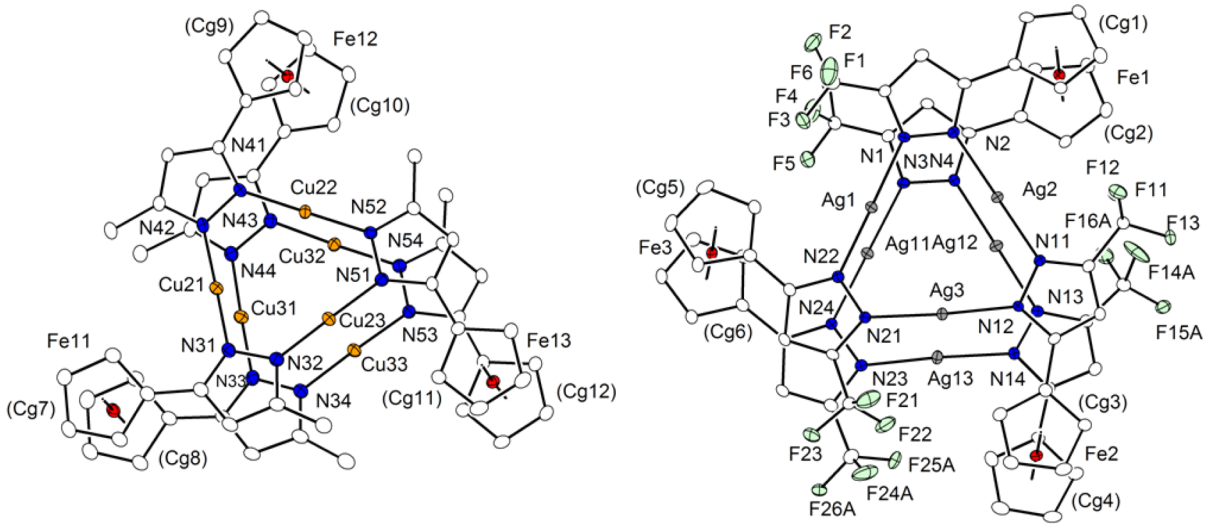

Figure 10. Plot (30% probability thermal ellipsoids) of the molecular structure of $Cu_6L_3^H$ (left, only one of the two crystallographically independent molecules is shown) and $Ag_6L_3^F$ (right). Hydrogen atoms and solvent molecules omitted for clarity).

corresponding to the $[M_6L_3]^+$ species is present, and in the case of $Ag_6L_3^F$, this is also the base peak of the spectrum. Furthermore, a less intense peak corresponding to $[M_7L_3]^+$ and relatively strong signals due to $[M_xL_2]^+$ (x = 3, 4, 5) are detected (Figure 8

DOI: 10.1021/acs.inorgchem.5b00898
Inorg. Chem. 2015, 54, 6917−6927

and Supporting Information, Figures S14 and S15). These observations suggest that the three complexes $[Cu_2L^H]_x$, $[Ag_2L^H]_x$, and $[Ag_2L^F]_x$ have a molecular structure composed of six M^I ions and three ferrocene-based pz ligands, which was later confirmed by X-ray crystallography (see below). The fourth compound, obtained from the reaction of $[Cu(MeCN)_4](BF_4)$ with H_2L^F, gives rise to a different MALDI mass spectrum (Figure 9 and Supporting Information, Figure S16). In this case the two most intense peaks correspond to species $[Cu_3L^F_2]^+$ and $[Cu_4L^F_2]^+$, while no signals originating from a complex ion with three ligands could be detected. The MALDI mass spectrum, together with the ^{1}H NMR results (see below), indicates the formation of a complex with different nuclearity in this case, identified as $Cu_4L^F_2$. When the protocol used for the synthesis of the above copper(I) and silver(I) complexes was extended to the higher homologue, gold(I), the corresponding hexanuclear $[Au_2L^R]_3$ compounds indeed form according to MALDI-TOF-MS analysis of the reaction mixtures. Unfortunately, however, the different solubility of the $[Au_2L^R]_x$ complexes has prevented, so far, the isolation of pure material. Efforts are underway to improve the synthetic strategy and the purification process for the missing members of this family of group 11 complexes.

Single crystals suitable for X-ray diffraction were obtained for two complexes, namely, $Cu_6L^H_3$ and $Ag_6L^F_3$. Their molecular structures are depicted in Figure 10 (further views as well as tables with bond lengths and angles are provided in the Supporting Information, Figures S25–S27). In both cases, the pz moieties form the common triangular M_3N_6 metalla-macrocycles. Because of the ferrocene clips, within each complex two of these almost planar metalla-macrocycles are parallel and stacked in an eclipsed conformation. This forces the metal ions to adopt the quite uncommon frontal mode arrangement.[21] The distances between two M^I ions within the triangular M_3N_6 metalla-macrocycles are in the range of 3.13–3.26 Å for $Cu_6L^H_3$ and 3.40–3.49 Å for $Ag_6L^F_3$; the $M^I\cdots M^I$ interplanar distances are in the ranges of 3.44–3.51 Å in the copper complex and 3.28–3.30 Å for the silver complex. Hence this kind of double-deck structure induces Ag···Ag ligand-supported contacts that are shorter than the sum of van der Waals radii of the single metal atoms, while in the case of copper(I) complexes those contacts are slightly longer than the sum of van der Waals radii (van der Waals radii are 1.40 Å for Cu and 1.72 Å for Ag).[36] $M^I\cdots M^I$ distances between the two triangular M_3N_6 decks are clearly shorter in $Ag_6L^F_3$ despite the identical ferrocene spacers that link the eclipsed pyrazole rings of each ligand (the Cp···Cp separation is ~3.3 Å for all ferrocene subunits), indicating significant closed-shell d^{10}–d^{10} interactions for Ag^I, as anticipated.[37−39] However, $Cu_6L^H_3$ crystallizes as an infinite chain of hexanuclear entities showing short (<4 Å) intermolecular Cu···Cu contacts, the shortest of which is 3.37 Å (Figure 11). Such ligand-unsupported $M^I\cdots M^I$ interactions are not present in the solid-state structure of $Ag_6L^F_3$ where all intermolecular Ag···Ag separations between hexanuclear molecules are >4.5 Å (Supporting Information, Figure S31). It can be concluded that, in solid state, *intra*molecular closed-shell d^{10}–d^{10} interactions are operative for $Ag_6L^F_3$, while *inter*molecular closed-shell d^{10}–d^{10} interactions dominate in the case of $Cu_6L^H_3$. It is interesting to note that, once the constraints imposed by the ligand are absent, metallophilic interactions mostly favor an offset "dimer of trimer" arrangement of the $[M(\mu\text{-pz})]_3$ rings where the N–M^I–N axes of the pairs of interacting two-coordinate coinage metal ions are perpendicular, not parallel (staggered with respect to the M–M axis; see **I**, Figure 1). This offset supramolecular arrangement, or its

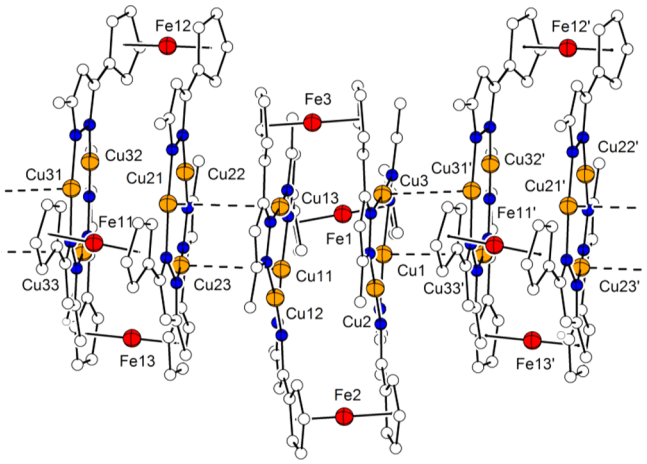

Figure 11. Plot of the structure of $Cu_6L^H_3$ emphasizing the arrangement of the molecules in the crystal with intermolecular Cu···Cu contacts <4 Å (dashed lines). Selected distances [Å]: Cu1···Cu33′ 3.7535(6), Cu3···Cu31′ 3.3714(6), Cu11···Cu23 3.5407(6), Cu13···Cu21 3.8918(6). Symmetry transformation used to generate equivalent atoms: (′) $-1+x$, y, z.

combination with the eclipsed mode,[21] is known to be the most favorable for dimers of trimeric $[M(\mu\text{-pz})]_3$ based on both theoretical calculations[7] and experimental observations.[5,9,10,12] One may assume that in $Ag_6L^F_3$ the more bulky CF_3 substituents induce larger distances between the molecules in solid state and thus prevent close *inter*molecular d^{10}–d^{10} contacts between perpendicular N–Ag^I–N pairs (staggered with respect to the Ag–Ag axis), leaving the less favored *intra*molecular d^{10}–d^{10} contacts between parallel N–Ag^I–N units (eclipsed with respect to the Ag–Ag axis) as the only alternative. In line with this interpretation, and in line with the greater strength of closed-shell d^{10}–d^{10} interactions in case of Ag^I compared to Cu^I, the solubility of $Ag_6L^H_3$ lacking the CF_3 substituents is very low, suggesting strong *inter*molecular d^{10}–d^{10} contacts that lead to a pseudopolymeric structure.

To further characterize the new ferrocene-based ligands and their oligonuclear Cu^I and Ag^I complexes, Mössbauer spectra of solid material were collected at 80 K; the spectrum of H_2L^H is shown in Figure 12 as an example. All spectra show a single quadrupole doublet with isomeric shift and quadrupole splitting parameters typical of low-spin Fe^{II} and values similar to those of the recently reported 4-ferrocenyl-3,5-dimethylpyrazole[40] and of ferrocene itself.[41] Neither the remote substituent on the pyrazole ring (CF_3 or Me) nor the nature of the coinage metal (Cu^I or Ag^I) affect significantly the Mössbauer spectra. The results obtained are summarized in Table 1.

^{1}H NMR spectroscopy of $Cu_6L^H_3$ and $Ag_6L^F_3$ suggests that the molecular structures described above are retained in solution; because of its extremely low solubility, characterization of $Ag_6L^H_3$ was not possible. In a hexanuclear structure $M_6L^R_3$ with C_{3h} symmetry the ferrocenyl protons 2-H^{Fc} and 5-H^{Fc}, as well as protons 3-H^{Fc} and 4-H^{Fc}, are inequivalent and should give distinct resonances. The ^{1}H NMR spectrum of $Cu_6L^H_3$ ($CDCl_3$, 298 K) shows only three signals in the Cp region, since 3-H^{Fc} and 4-H^{Fc} are accidentally isochronous (at 4.33 ppm), probably because of the similarity of their environment. However, the chemical shifts of 2-H^{Fc} (the one closest to the Cu_3N_6 metallamacrocycle) and 5-H^{Fc} are, as expected, very different (5.62 vs 4.55 ppm), the one for 2-H^{Fc} appearing at rather low

DOI: 10.1021/acs.inorgchem.5b00898
Inorg. Chem. 2015, 54, 6917–6927

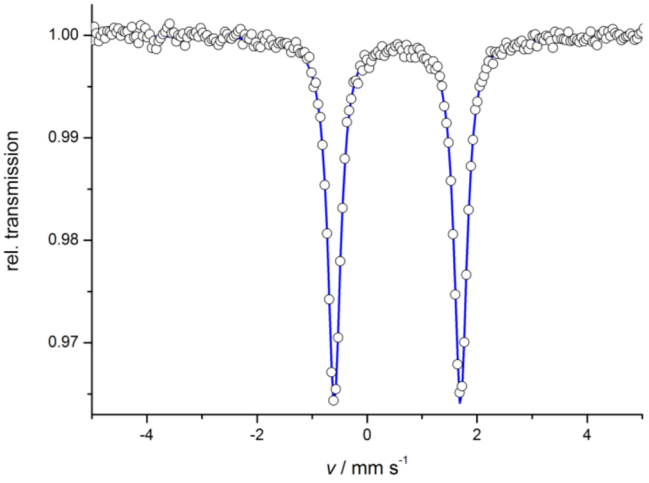

Figure 12. Mössbauer spectrum of solid H_2L^H at 80 K; the blue line represents a simulation with δ = 0.55 mm s^{-1} and quadrupole splitting ΔE_Q = 2.30 mm s^{-1}.

Table 1. Mössbauer Parameters [mm s^{-1}] of the Proligands and Complexes at 80 K in Solid State

	H_2L^H	H_2L^F	$Cu_6L_3^H$	$Ag_6L_3^H$	$Cu_4L_2^F$	$Ag_6L_3^F$
δ	0.55	0.54	0.53	0.54	0.54	0.53
ΔE_Q	2.30	2.29	2.26	2.30	2.31	2.26

field due to its proximity to a metal center (Supporting Information, Figure S6).

The ^{1}H NMR spectrum of $Ag_6L_3^F$ in DMF-d_7 shows the same pattern of three Cp resonances with those for 3-H^{Fc} and 4-H^{Fc} being accidentally isochronous (at 4.51 ppm), while in toluene-d_8 3-H^{Fc} and 4-H^{Fc} give separate peaks (Supporting Information, Figure S7). A possible explanation for the solvent dependence could be the well-known formation of π acid−π base adducts between trimeric Ag_3N_6 metallamacrocycles of fluorinated pyrazole ligands and toluene,[16] which could induce a more asymmetric electronic distribution and thus lead to a splitting of the 3-H^{Fc}/4-H^{Fc} signals.

As expected from its MALDI-TOF mass spectrum, $Cu_4L^F{}_2$ behaves differently. Its ^{1}H NMR spectrum ($CDCl_3$, 298 K) shows two signals for the pyrazole protons 4-H^{pz} and two additional signals for the 2-H^{Fc} protons in a one-to-one ratio (Supporting Information, Figure S8). On the basis of the similarity of the ^{1}H NMR spectrum with the spectra measured for H_2L^H/H_2L^F at low temperatures, and in view of the MALDI-TOF-MS results, formation of a structure with C_2 symmetry resembling that of H_2L^H in the solid state (Figure 2) is proposed in which the four protons responsible of the N−H···N hydrogen bonds are replaced by Cu^I ions. In such structure the two 4-H^{pz} and the two 2-H^{Fc} protons of each ligand are diastereotopic. Similar to what was found for H_2L^F, however, the presence of more species in equilibrium, besides $Cu_4L^F{}_2$, cannot be excluded: VT ^{1}H NMR spectroscopy shows, in fact, additional minor peaks that rise when the sample is cooled (Supporting Information, Figure S9). The low intensity of these signals, together with the low solubility of the compound, prevents further investigations to unravel the identity of the additional species. However, the presence of, and equilibria between, coinage-pyrazolato species with different nuclearity in solution have previously been reported.[12,42]

Redox properties of the complexes, with the exception of $Ag_6L_3^H$ because of its insolubility, were investigated by cyclic voltammetry in DMF and PhCN solutions. All three complexes undergo some redox processes in the range from −0.1 to +0.3 V versus Fc/Fc^+, which are assigned to the ferrocene units in the ligand scaffolds. In DMF, both copper complexes show a rather broad and irreversible anodic process with E_p^a = +105 mV for $Cu_6L_3^H$ and E_p^a = +182 mV for $Cu_4L_2^F$ (at a scan rate of 100 mV s^{-1}). The CV of $Ag_6L_3^F$ in DMF appears different, and both anodic and cathodic responses in the forward and reverse scans, respectively, are clearly present. The oxidation wave is composed by three subprocesses, which is also reflected in the square wave voltammogram (SWV, Supporting Information, Figure S12). While it may be tempting to attribute these three waves to sequential oxidations of the three ferrocene subunits in $Ag_6L_3^F$, the single reduction wave in the cathodic backscan indicates a more complicated scenario possibly involving fragmentation of the $Ag_6L_3^F$ core after the third oxidation. In PhCN solution the electrochemical processes are more well-behaved and show characteristics for quasi-reversibility or even reversibility (Figure 13 and Supporting Information, Figure S13). In general, anodic waves associated with oxidation of the ferrocene units appear broad and are probably composed of several closely spaced processes. Compared with the free proligands, oxidations occur at higher potentials in the copper complexes (E_p^a = +178 mV for $Cu_6L_3^H$ and +305 mV for $Cu_4L_2^F$; all at scan rate 100 mV s^{-1}) but at lower potential in the case of $Ag_6L_3^F$ (E_p^a = 184 mV).

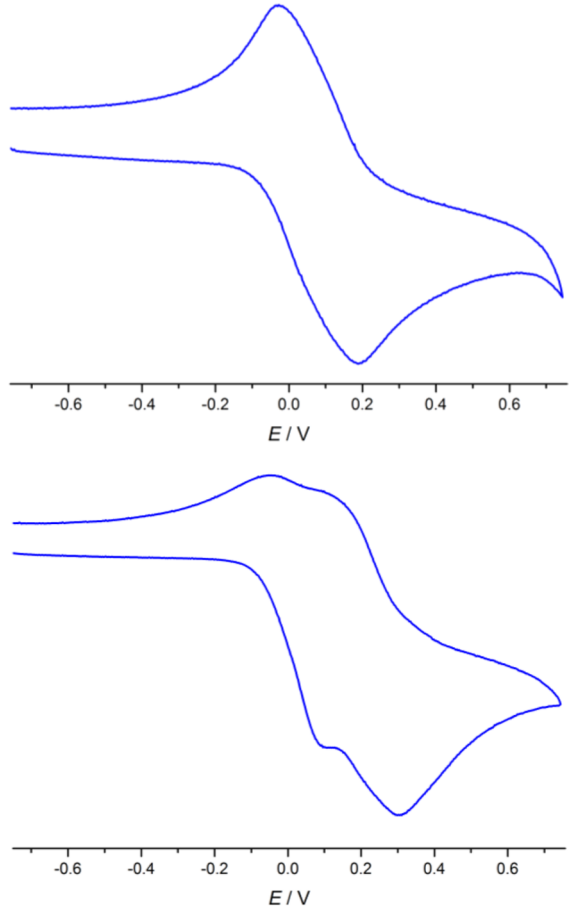

Figure 13. Cyclic voltammograms of $Cu_6L_3^H$ (upper) and $Cu_4L_2^F$ (lower) in PhCN/0.1 M [nBu$_4$N]PF_6 vs Fc/Fc^+ at a scan rate of 100 mV s^{-1}; potentials are given in volts vs the Fc/Fc^+ couple.

DOI: 10.1021/acs.inorgchem.5b00898
Inorg. Chem. 2015, 54, 6917−6927

A preliminary screening of the photoluminescence properties of all four complexes was performed. In solid state (powder samples) upon excitation with UV light (350−370 nm), a weak emission in the visible region (at ∼420−440 nm) was recorded for the four complexes (Figure 14 and Supporting Information, Figures S18−S20). Since all spectra show a similar pattern it can be concluded that luminescence of these prismatic hexanuclear complexes is not significantly influenced, neither by the nature of the coinage metal ions nor by the substituent on the pyrazole rings. To understand the origin of the luminescence, photophysical properties of the two proligands were recorded under the same conditions. Both H_2L^H and H_2L^F show a very weak emission centered at 400−420 nm, that is, in the same range as the complexes (Supporting Information, Figures S21 and S22), indicating that the emissions are mainly ligand-centered. It is, however, feasible that also the intra- and intermolecular contacts between the d^{10} closed-shell metal ions contribute, to some extent, to the photoluminescence.

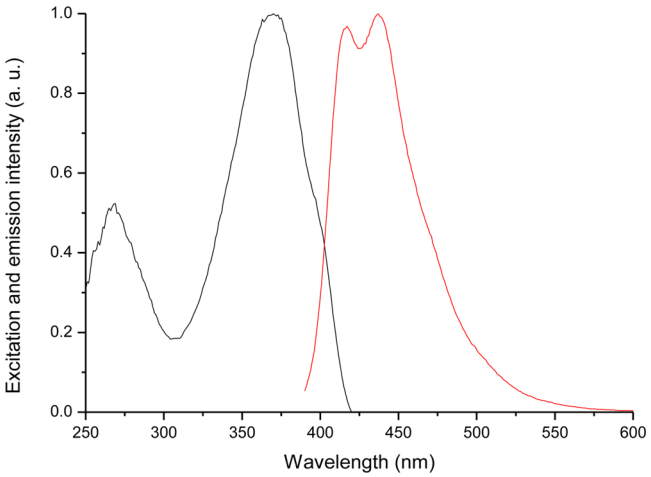

Figure 14. Photoluminescence spectra of $Cu_6L_3^H$. The emission spectrum (red) was detected after excitation at 370 nm, while the excitation spectrum (black) monitored the emission at 435 nm.

CONCLUSIONS

In this work two new ferrocene-based pyrazole ligands H_2L^H and H_2L^F are reported that feature two parallel and eclipsed pyrazole rings linked by a ferrocene clip. In solid state these proligands form different types of dimeric aggregates via four intermolecular N−H···N hydrogen bonds, with crystallographic C_2 or non-crystallographic C_{2h} symmetry. Dimers are also present in solution at low temperatures, though the C_2 isomer featuring a central ring of four pyrazoles, which is a common motif for pyrazoles, dominates in both cases. With Cu^I and Ag^I ions these ligands mostly give hexanuclear complexes that feature two stacked M_3N_6 metalla-macrocyles; these have been characterized crystallographically in the cases of $Cu_6L_3^H$ and $Ag_6L_3^F$. Their overall structure of (noncrystallographic) C_{3h} symmetry, with three ferrocene clips linking the two metalla-macrocycles, enforces a quite uncommon frontal mode arrangement of the M_3N_6 decks. Inspection of the $M^I\cdots M^I$ distances in solid state indicates three *intra*molecular d^{10}−d^{10} interactions between the two decks only for the silver(I) complex but *inter*molecular d^{10}−d^{10} contacts for $Cu_6L_3^H$. As an exception, for the combination Cu^I/H_2L^F the preferred oligomeric form seems to be the tetracopper dimer $Cu_4L_2^F$ with molecular C_2 symmetry, according to MALDI-TOF MS and NMR data; its structure is most likely similar to the structures of both proligands in solution and H_2L^H in solid state. While the different pyrazole substituents in H_2L^H and H_2L^F, specifically, Me or CF_3 groups, have little influence on the Mössbauer parameters and luminescene properties of the double-decker $M_6L_3^R$ complexes, they clearly effect the redox potentials of the ferrocene moieties.

The present systems demonstrate a new strategy of controlling the stacking of two planar trinuclear M_3N_6 metalla-macrocyles in rather rigid arrangements. It will be interesting to study the effect of slight modification of the intramolecular distance of the two M_3N_6 decks by, for example, using other metallocene clips, or by oxidation of the ferrocene units.

EXPERIMETAL SECTION

Methods and Materials. All ligand syntheses were performed under an anaerobic and anhydrous atmosphere of dry argon by using standard Schlenk techniques. 1,1′-Bisacetylferrocene was prepared according to a literature procedure.[32] EtOH was dried over sodium; tetrahydrofuran (THF) was dried over sodium in the presence of benzophenone; PhCN was dried over P_2O_5; MeOH, CH_2Cl_2, and DMF were dried over CaH_2; all solvents were distilled prior to use. ***Caution!*** *Toxic and hazardous compounds such as hydrazine must be handled with proper precautions.* NMR spectra were recorded on Bruker Avance 300 and 400 spectrometers. Chemical shifts are reported in parts per million relative to residual proton and carbon signals of the solvent ($CDCl_3$, δ_H = 7.26, δ_C = 77.16 ppm; CD_2Cl_2, δ_H = 5.32, δ_C = 53.84; DMSO-d_6, δ_H = 2.50, δ_C = 39.52; toluene-d_8, δ_H = 2.08, δ_C = 20.43; DMF-d_7, δ_H = 2.75, δ_C = 29.76). Electron ionization (EI) mass spectra were recorded with a Finnigan MAT 8200 and MALDI-TOF mass spectra with a Bruker Autoflex Speed. CV and SWV were measured with a PerkinElmer 263A potentiostat controlled by electrochemistry powersuit software. Mössbauer spectra were recorded with a ^{57}Co source in a Rh matrix using an alternating constant acceleration Wissel Mössbauer spectrometer operated in the transmission mode and equipped with a Janis closed-cycle helium cryostat. Isomer shifts are given relative to iron metal at ambient temperature. Luminescence spectra were recorded using a Horiba−Jobin−Yvon Fluorolog-3 instrument, equipped with an R928 photomultiplier tube from Hamamatsu and a 450 W Xe lamp as an excitation source. Elemental analyses were performed by the analytical laboratory of the Institute of Inorganic Chemistry at Georg-August-University using an Elementar Vario EL III instrument.

X-ray Crystallography. Crystal data and details of the data collections are given in the Supporting Information (Table S2). X-ray data were collected on a STOE IPDS II diffractometer (graphite monochromated Mo Kα radiation, λ = 0.710 73 Å) by use of ω scans at −140 °C. The structures were solved by direct methods (SHELXS-2013) and refined on F^2 using all reflections with SHELXL-2013.[43] Most non-hydrogen atoms were refined anisotropically. Most hydrogen atoms were placed in calculated positions and assigned to an isotropic displacement parameter of 1.2/1.5 U_{eq}(C). The positional parameters of the nitrogen bound hydrogen atoms in H_2L^H and H_2L^F were refined freely. A fixed isotropic displacement parameter of 0.08 Å^2 was assigned in case of H_2L^H. In H_2L^H the hydrogen atoms were found to be disordered about the two nitrogen atoms of the pyrazole moiety (occupancy factors: 0.49(4)/0.51(4) and 0.46(4)/0.54(4)). Et_2O solvent molecules were found to be disordered over centers of inversion in $Cu_6L_3^H$. One of the two solvent molecules shows in addition a positional disorder (occupancy factors: 0.298(9)/ 0.202(9)). DFIX restraints (d_{C-O} = 1.43 Å and d_{C-C} = 1.51 Å) were used to model the disorder. Atoms of the disordered solvent molecules were refined isotropically. In $Ag_6L_3^F$ the F atoms of two CF_3 groups were found to be disordered about two (occupancy factors: 0.699(8)/0.301(8)) and three positions. In case of the second disordered group the occupancy factors were fixed at 0.25, 0.25, and 0.50. SADI restraints (d_{C-F} and d_{F-F}) and EADP constraints were used to model the disorder. Face-indexed absorption corrections were performed numerically with the program X-RED.[44]

DOI: 10.1021/acs.inorgchem.5b00898
Inorg. Chem. 2015, 54, 6917−6927

1,1′-Bis(acetoacetyl)ferrocene (I^H) and 1,1′-Bis-(trifluoroacetoacetyl)ferrocene (I^F). The synthesis was adapted from the literature method.[33] Na (900 mg, 39.1 mmol, 2.1 equiv) was treated with dry EtOH (10 mL), and the suspension was stirred until all sodium had disappeared. The solvent was then removed under reduced pressure, and the obtained NaOEt was dried for 30 min in vacuo. It was then suspended in dry THF (20 mL) and 1,1′-bis(acetyl)ferrocene (5.0 g, 18.5 mmol, 1.0 equiv) and the appropriate ester (3.4 g, 38.6 mmol, 2.1 equiv of ethyl acetate for I^H; 5.5 g, 38.7 mmol, 2.1 equiv of ethyl trifluoroacetate for I^F) was added. The resulting mixture was stirred, heated at 50 °C overnight, then cooled to room temperature, and filtered. The solid was washed with small portions of Et_2O and then poured into water (20 mL), and the aqueous mixture was then acidified with AcOH. The resulting solid product was separated by filtration and dried in vacuo.

I^H. Yield 2.2 g, 6.2 mmol, 34%. Spectroscopic data were in agreement with reported values.[33]

I^F. Yield 5.9 g, 12.8 mmol, 69%. ^{1}H NMR ($CDCl_3$, 300 MHz): δ [ppm] = 4.67 (t, 4H, 2,5-H^{Fc}), 4.89 (t, 4H, 3,4-H^{Fc}), 6.02 (s, 2H, CH). ^{19}F NMR ($CDCl_3$, 282 MHz): δ [ppm] = −76.14.

1,1′-Bis(5-methyl-1H-pyrazol-3-yl)ferrocene (H_2L^H). I^H (2.1 g, 5.3 mmol, 1.0 equiv) was dissolved in EtOH (40 mL), and hydrazine monohydrate (1.78 g, 35.6 mmol, 6.0 equiv) was added dropwise; then AcOH (1 mL) was added. The mixture was heated to reflux for 2 h, and then the solvent was removed under reduced pressure. The residue was taken up with water (20 mL), separated by filtration, and dried in vacuo to give an orange-brown solid (yield 1.8 g, 5.2 mmol, 88%). Crystals suitable for X-ray diffraction were obtained by vapor diffusion of Et_2O in a solution of the crude material in CH_2Cl_2. ^{1}H NMR (DMSO-d_6, 300 MHz): δ [ppm] = 2.18 (s, 6H, CH_3), 4.08 (s, 4H, 3,4-H^{Fc}), 4.46 (s, 4H, 2,5-H^{Fc}), 5.96 (s, 2H, CH^{pz}), 12.26 (b, 2H, NH). ^{13}C NMR (DMSO-d_6, 75 MHz): 11.9 (CH_3), 67.2 (2,5-C^{Fc}), 69.6 (3,4-C^{Fc}), 101.5 (4-C^{pz}); quaternary carbon atoms could not be detected. ^{1}H NMR ($CDCl_3$, 300 MHz): δ [ppm] = 2.26 (s, 6H, CH_3), 4.18 (s, 4H, 3,4-H^{Fc}), 4.62 (s, 4H, 2,5-H^{Fc}), 5.72 (s, 2H, CH^{pz}). ^{1}H NMR (CD_2Cl_2, 400 MHz): δ [ppm] = 2.25 (s, 6H, CH_3), 4.20 (t, J = 1.6 Hz, 4H, 3,4-H^{Fc}), 4.61 (t, J = 1.6 Hz, 4H, 2,5-H^{Fc}), 5.74 (s, 2H, CH^{pz}). MS (EI): m/z (%) = 346.1 [M] (100). Anal. Calcd (%) for $C_{18}H_{18}FeN_4$: C, 62.45; H, 5.24; N, 16.18. Found: C, 62.41; H, 5.15; N, 15.90.

1,1′-Bis(5-trifluoromethyl-1H-pyrazol-3-yl)ferrocene (H_2L^F). I^F (5.0 g, 10.8 mmol, 1.0 equiv) was dissolved in EtOH (40 mL), and hydrazine monohydrate (3.25 g, 64.9 mmol, 6.0 equiv) was added dropwise; the reaction mixture was heated to reflux overnight. All solvent was then removed under reduced pressure, and the residue was taken up in aqueous HCl (2 M, 30 mL). The resulting mixture was placed in an ultrasonic bath for 15 min and then filtered, and the solid was dried in vacuo to give an orange-brown material (yield 2.47 g, 5.44 mmol, 50%). Crystals suitable for X-ray diffraction were obtained by slow evaporation of a solution of the crude product in CD_2Cl_2. ^{1}H NMR (DMSO-d_6, 300 MHz): δ [ppm] = 4.31 (s, 4H, 3,4-H^{Fc}), 4.74 (s, 4H, 2,5-H^{Fc}), 6.51 (s, 2H, CH^{pz}), 13.44 (b, 2H, NH). ^{13}C NMR (DMSO-d_6, 75 MHz): 46.5 (2,5-C^{Fc}), 70.3 (3,4-C^{Fc}), 74.2 (1-C^{Fc}), 99.9 (4-C^{pz}), 121.7 (q, $^1J_{C-F}$ = 266 Hz, CF_3), 141.4 (q, $^2J_{C-F}$ = 37 Hz, 5-C^{pz}), 141.5 (3-C^{pz}). ^{19}F NMR (DMSO-d_6, 282 MHz): −60.40. ^{1}H NMR ($CDCl_3$, 300 MHz): 4.34 (s, 4H, 3,4-H^{Fc}), 4.67 (s, 4H, 2,5-H^{Fc}), 6.30 (s, 2H, CH^{pz}). ^{19}F NMR ($CDCl_3$, 282 MHz): −61.88. ^{1}H NMR (CD_2Cl_2, 400 MHz): 4.36 (s, 4H, 3,4-H^{Fc}), 4.96 (s, 4H, 2,5-H^{Fc}), 6.35 (s, 2H, CH^{pz}). ^{19}F NMR (CD_2Cl_2, 376 MHz): −62.17. MS (EI): m/z (%) = 454.1 [M] (100). Anal. Calcd (%) for $C_{18}H_{12}F_6FeN_4$: C, 47.60; H, 2.66; N, 12.34. Found: C, 47.20; H, 2.76; N, 12.52.

$Cu_6L_3^H$. H_2L^H (50 mg, 0.144 mmol, 1.0 equiv) and [Cu(MeCN)$_4$]-(BF_4) (91 mg, 0.289 mmol, 2.0 equiv) were dissolved in dry MeOH (4 mL), and after 3 min, degassed Et_3N (0.1 mL, 0.717 mmol, 5.0 equiv) was added dropwise. A suspension immediately formed. The reaction mixture was stirred for 1 h and then filtered, and the resulting solid was washed with small amounts of MeOH. The product was dried in vacuo (yield 47 mg, 0.033 mmol, 69%). Crystals suitable for X-ray diffraction were obtained by vapor diffusion of Et_2O into a solution of the complex in DMF. ^{1}H NMR ($CDCl_3$, 400 MHz): δ [ppm] = 2.43 (s, 6H, CH_3), 4.33 (s, 4H, 3,4-H^{Fc}), 4.55 (s, 2H, 5-H^{Fc}), 5.62 (s, 2H, 2-H^{Fc}), 5.75 (s, 2H, CH^{pz}). MS (MALDI-TOF): m/z (%) = 734.9 (13), 763.1 (10), 800.0 (9), 827.0 (100), 879.0 [Cu_3L_2] (34), 941.9 [Cu_4L_2] (78), 1004.9 [Cu_5L_2] (39), 1234.0 (3), 1296.9 (4), 1413.9 [Cu_6L_3] (24), 1476.8 [Cu_7L_3] (3). Anal. Calcd (%) for $C_{54}H_{48}Cu_6Fe_3N_{12}$·0.5 Et_2O: C, 46.36; H, 3.68; N, 11.58. Found: C, 46.55; H, 3.71; N, 11.65.

$Ag_6L_3^H$. H_2L^H (50 mg, 0.144 mmol, 1.0 equiv) was suspended in a MeCN/MeOH 3:1 mixture (20 mL), and a solution of $AgBF_4$ (56 mg, 0.288 mmol, 2.0 equiv) in MeCN (2 mL) was added. After 3 min, Et_3N (0.1 mL, 0.717 mmol, 5.0 equiv) was added dropwise, causing immediate formation of a precipitate. The mixture was stirred for 30 min, and then the solid was separated by filtration, washed with small amounts of MeCN and MeOH, and dried in vacuo (yield 62 mg, 0.037 mmol, 77%). MS (MALDI-TOF): m/z (%) = 745.1 (100), 847.2 (71), 958.9 (46), 1061.0 (29), 1119.9 [Ag_4L_2] (26), 1226.8 [Ag_5L_2] (21), 1412.9 (7), 1518.8 (12), 1679.8 [Ag_6L_3] (15), 1786.7 [Ag_7L_3] (13).

$Cu_4L_2^F$. H_2L^F (150 mg, 0.330 mmol, 1.0 equiv) and [Cu(MeCN)$_4$]-(BF_4) (208 mg, 0.661 mmol, 2.0 equiv) were dissolved in dry MeOH (4 mL), and after 3 min, degassed Et_3N (0.2 mL, 1.43 mmol, 4.3 equiv) was added dropwise, causing immediate formation of a suspension. The mixture was stirred for 1 h and then filtered, and the solid was washed with small amounts of MeOH. The resulting product was dried in vacuo (yield 105 mg, 0.091 mmol, 55%). ^{1}H NMR ($CDCl_3$, 400 MHz): δ [ppm] = 4.36 (s, 2H, 3-H^{Fc}), 4.40 (s, 2H, 4-H^{Fc}), 4.62 (s, 2H, 5-H^{Fc}) 5.28 (s, 1H, 2-H^{Fc}), 5.35 (s, 1H, 2-H$^{Fc'}$), 6.30 (s, 1H, CH^{pz}), 6.36 (s, 1H, CH$^{pz'}$). ^{19}F NMR ($CDCl_3$, 376 MHz): −61.29 (t, J = 4.4 Hz), −61.34 (t, J = 4.4 Hz). MS (MALDI-TOF): m/z (%) = 1094.8 [Cu_3L_2] (100), 1157.7 [Cu_4L_2] (18). Anal. Calcd (%) for $C_{36}H_{20}Cu_4F_{12}Fe_2N_8$: C, 37.32; H, 1.74; N, 9.67. Found: C, 37.33; H, 2.13; N, 9.69.

$Ag_6L_3^F$. H_2L^F (100 mg, 0.220 mmol, 1.0 equiv) was suspended in MeCN (5 mL), and a solution of $AgBF_4$ (86 mg, 0.442 mmol, 2.0 equiv) in MeCN (2 mL) was added. After 3 min, Et_3N (0.1 mL, 0.717 mmol, 3.3 equiv) was added dropwise, causing immediate formation of a precipitate. The mixture was stirred for 30 min, and then the solid was separated by filtration, washed with small amounts of MeCN, and dried in vacuo (yield 118 mg, 0.059 mmol, 80%). Crystals suitable for X-ray diffraction were obtained by vapor diffusion of MeOH into a solution of the complex in DMF. ^{1}H NMR (toluene-d_8, 300 MHz): δ [ppm] = 4.09 (s, 2H, 4-H^{Fc}), 4.24 (s, 2H, 5-H^{Fc}), 4.36 (s, 2H, 3-H^{Fc}), 5.53 (s, 2H, 2-H^{Fc}), 6.25 (s, 2H, CH^{pz}). ^{13}C NMR (toluene-d_8, 75 MHz): 66.6 (2-C^{Fc}), 68.1 (5-C^{Fc}), 69.5, 69.6 (3-C^{Fc}, 4-C^{Fc}), 79.5 (1-C^{Fc}), 103.2 (4-C^{pz}); the other carbon atoms could not be detected. ^{19}F NMR (toluene-d_8, 282 MHz): −58.79. ^{1}H NMR (DMF-d_7, 300 MHz): 4.51 (s, 4H, 3,4-H^{Fc}), 4.94 (s, 2H, 5-H^{Fc}), 5.52 (s, 2H, 2-H^{Fc}), 6.68 (s, 2H, CH^{pz}). ^{13}C NMR (DMF-d_7, 100 MHz): 66.2 (2-C^{Fc}), 68.3 (5-C^{Fc}), 69.0, 69.5 (3-C^{Fc}, 4-C^{Fc}), 80.0 (1-C^{Fc}), 103.2 (4-C^{pz}), 122.0 (q, $^1J_{C-F}$ = 267 Hz, CF_3), 143.0 (b, 5-C^{pz}), 149.4 (3-C^{pz}). ^{19}F NMR (DMF-d_7, 376 MHz): −59.05. MS (MALDI-TOF): m/z (%) = 1028.7 (11), 1227.8 [Ag_3L_2] (30), 1335.7 [Ag_4L_2] (70), 1442.6 [Ag_5L_2] (11), 2003.4 [Ag_6L_3] (100), 2110.3 [Ag_7L_3] (7). Anal. Calcd (%) for $C_{54}H_{30}Ag_6F_{18}Fe_3N_{12}$: C, 32.37; H, 1.51; N, 8.39. Found: C, 31.98; H, 1.80; N, 8.39.

■ ASSOCIATED CONTENT

Ⓢ Supporting Information

Selected NMR spectra; MALDI-TOF mass spectra; cyclic voltammograms; luminescence spectra of [M_2L^R]$_x$ species; crystallographic details (CIF) and ORTEP plots. The Supporting Information is available free of charge on the ACS Publications website at DOI: 10.1021/acs.inorgchem.5b00898.

■ AUTHOR INFORMATION

Corresponding Author

*E-mail: franc.meyer@chemie.uni-goettingen.de.

Notes

The authors declare no competing financial interest.

DOI: 10.1021/acs.inorgchem.5b00898
Inorg. Chem. 2015, 54, 6917−6927

■ ACKNOWLEDGMENTS

We thank Dr. M. John for collecting the ^{19}F COSY spectrum of H_2L^F. Financial support by the Georg-August-University is gratefully acknowledged.

■ REFERENCES

(1) La Monica, G.; Ardizzoia, G. A. *Prog. Inorg. Chem.* **1997**, *46*, 151.
(2) Mohamed, A. A. *Coord. Chem. Rev.* **2010**, *254*, 1918.
(3) Halcrow, M. A. *Dalton Trans.* **2009**, 2059.
(4) Fujisawa, K.; Ishikawa, Y.; Miyashita, Y.; Okamoto, K.-i. *Inorg. Chim. Acta* **2010**, *363*, 2977.
(5) Dias, H. V. R.; Diyabalanage, H. V. K.; Eldabaja, M. G.; Elbjeirami, O.; Rawashdeh-Omary, M. A.; Omary, M. A. *J. Am. Chem. Soc.* **2005**, *127*, 7489.
(6) Vorontsov, I.; Kovalevsky, A.; Chen, Y.-S.; Graber, T.; Gembicky, M.; Novozhilova, I.; Omary, M.; Coppens, P. *Phys. Rev. Lett.* **2005**, *94*, 193003.
(7) Grimes, T.; Omary, M. A.; Dias, H. V. R.; Cundari, T. R. *J. Phys. Chem. A* **2006**, *110*, 5823.
(8) Yang, G.; Raptis, R. G. *Inorg. Chem.* **2003**, *42*, 261.
(9) Omary, M. A.; Rawashdeh-Omary, M. A.; Gonser, M. W. A.; Elbjeirami, O.; Grimes, T.; Cundari, T. R.; Diyabalanage, H. V. K.; Gamage, C. S. P.; Dias, H. V. R. *Inorg. Chem.* **2005**, *44*, 8200.
(10) Zhang, J.-X.; He, J.; Yin, Y.-G.; Hu, M.-H.; Li, D.; Huang, X.-C. *Inorg. Chem.* **2008**, *47*, 3471.
(11) Jahnke, A. C.; Pröpper, K.; Bronner, C.; Teichgräber, J.; Dechert, S.; John, M.; Wenger, O. S.; Meyer, F. *J. Am. Chem. Soc.* **2012**, *134*, 2938.
(12) Veronelli, M.; Kindermann, N.; Dechert, S.; Meyer, S.; Meyer, F. *Inorg. Chem.* **2014**, *53*, 2333.
(13) Singh, K.; Long, J. R.; Stavropoulos, P. *J. Am. Chem. Soc.* **1997**, *119*, 2942.
(14) Meyer, F.; Jacobi, A.; Zsolnai, L. *Chem. Ber./Recl.* **1997**, *130*, 1441.
(15) Mohamed, A. A.; Pérez, L. M.; Fackler, J. P. *Inorg. Chim. Acta* **2005**, *358*, 1657.
(16) Dias, H. V. R.; Gamage, C. S. P.; Keltner, J.; Diyabalanage, H. V. K.; Omari, I.; Eyobo, Y.; Dias, N. R.; Roehr, N.; McKinney, L.; Poth, T. *Inorg. Chem.* **2007**, *46*, 2979.
(17) Yang, G.; Baran, P.; Martínez, A. R.; Raptis, R. G. *Cryst. Growth Des.* **2013**, *13*, 264.
(18) Hettiarachchi, C. V.; Rawashdeh-Omary, M. A.; Korir, D.; Kohistani, J.; Yousufuddin, M.; Dias, H. V. R. *Inorg. Chem.* **2013**, *52*, 13576.
(19) Ni, W.-X.; Qiu, Y.-M.; Li, M.; Zheng, J.; Sun, R. W.-Y.; Zhan, S.-Z.; Ng, S. W.; Li, D. *J. Am. Chem. Soc.* **2014**, *136*, 9532.
(20) Jozak, T.; Sun, Y.; Schmitt, Y.; Lebedkin, S.; Kappes, M.; Gerhards, M.; Thiel, W. R. *Chem.—Eur. J.* **2011**, *17*, 3384.
(21) Gao, G.-F.; Li, M.; Zhan, S.-Z.; Lv, Z.; Chen, G.-h.; Li, D. *Chem.—Eur. J.* **2011**, *17*, 4113.
(22) Duan, P.-C.; Wang, Z.-Y.; Chen, J.-H.; Yang, G.; Raptis, R. G. *Dalton Trans.* **2013**, *42*, 14951.
(23) Horikoshi, R. *Coord. Chem. Rev.* **2013**, *257*, 621.
(24) Braga, D.; Polito, M.; Bracaccini, M.; D'Addario, D.; Tagliavini, E.; Sturba, L.; Grepioni, F. *Organometallics* **2003**, *22*, 2142.
(25) Horikoshi, R.; Nambu, C.; Mochida, T. *New J. Chem.* **2004**, *28*, 26.
(26) Mochida, T.; Shimizu, F.; Shimizu, H.; Okazawa, K.; Sato, F.; Kuwahara, D. *J. Organomet. Chem.* **2007**, *692*, 1834.
(27) Hauser, C. R.; Cain, C. E. *J. Org. Chem.* **1958**, *23*, 1142.
(28) Cain, C. E.; Mashburn, T. A.; Hauser, C. R. *J. Org. Chem.* **1961**, *26*, 1030.
(29) Schlögl, K.; Egger, H. *Monatsh. Chem.* **1963**, *94*, 1054.
(30) Thiel, W. R.; Priermeier, T.; Fiedler, D. A.; Bond, A. M.; Mattner, M. R. *J. Organomet. Chem.* **1996**, *514*, 137.
(31) Verma, G. K.; Verma, R. K.; Singh, M. S. *RSC Adv.* **2013**, *3*, 245.
(32) Zhao, Y.-C.; Zhou, D.; Chen, Q.; Zhang, X.-J.; Bian, N.; Qi, A.-D.; Han, B.-H. *Macromolecules* **2011**, *44*, 6382.
(33) Yan, C.-G.; Zhu, M.-J.; Sun, J.; Liu, W.-L.; Shi, Y.-C. *J. Coord. Chem.* **2007**, *60*, 1083.
(34) Dias, H. V. R.; Diyabalanage, H. V. K. *Polyhedron* **2006**, *25*, 1655.
(35) Connelly, N. G.; Geiger, W. E. *Chem. Rev.* **1996**, *96*, 877.
(36) Bondi, A. *J. Phys. Chem.* **1964**, *68*, 441.
(37) Magnko, L.; Schweizer, M.; Rauhut, G.; Schütz, M.; Stoll, H.; Werner, H.-J. *Phys. Chem. Chem. Phys.* **2002**, *4*, 1006.
(38) Jansen, M. *Angew. Chem., Int. Ed. Engl.* **1987**, *26*, 1098.
(39) Schmidbaur, H.; Schier, A. *Angew. Chem., Int. Ed.* **2015**, *54*, 746.
(40) Tampier, S.; Bleifuss, S. M.; Abd-Elzaher, M. M.; Sutter, J.; Heinemann, F. W.; Burzlaff, N. *Organometallics* **2013**, *32*, 5935.
(41) Watanabe, M.; Sano, H. *Bull. Chem. Soc. Jpn.* **1990**, *63*, 777.
(42) Krishantha, D. M. M.; Gamage, C. S. P.; Schelly, Z. A.; Dias, H. V. R. *Inorg. Chem.* **2008**, *47*, 7065.
(43) Sheldrick, G. M. *Acta Crystallogr.* **2008**, *A64*, 112.
(44) *X-RED;* STOE & CIE GmbH: Darmstadt, Germany, 2002.

DOI: 10.1021/acs.inorgchem.5b00898
Inorg. Chem. 2015, 54, 6917−6927